Interactions of the Antimicrobial Peptides Temporins with Model Biomembranes. Comparison of Temporins B and L[†]

Hongxia Zhao,[‡] Andrea C. Rinaldi,[§] Antonio Di Giulio,[||] Maurizio Simmaco,[⊥] and Paavo K. J. Kinnunen*,[‡]

Helsinki Biophysics & Biomembrane Group, Institute of Biomedicine, University of Helsinki, Finland, Dipartimento di Scienze Mediche Internistiche, Università di Cagliari, Monserrato (CA), Italy, Dipartimento di Scienze e Tecnologie Biomediche, Università dell'Aquila, L'Aquila, Italy, and Dipartimento di Scienze Biochimiche "A. Rossi Fanelli" and CNR, Centro di Biologia Molecolare, Università "La Sapienza", Rome, Italy

Received October 15, 2001; Revised Manuscript Received January 18, 2002

ABSTRACT: Temporins are short (10−13 amino acids) and linear antimicrobial peptides first isolated from the skin of the European red frog, *Rana temporaria*, and are effective against Gram-positive bacteria and *Candida albicans*. To get insight into their mechanism(s) of action, we compared the effects on model membranes exerted by two members of this family, viz., temporin B (LLPIVGNLLKSLL-NH_2) and temporin L (FVQWFSKFLGRIL-NH_2). More specifically, we measured their insertion into lipid monolayers as well as their effects on the structural dynamics of liposomal bilayers as revealed by diphenylhexatriene (DPH)- and pyrene-labeled phospholipids. We also observed the impact of these peptides on the topology of giant vesicles. Both temporins readily penetrate into lipid monolayers, their intercalation being enhanced in the presence of the common bacterial negatively charged phospholipid phosphatidylglycerol. Instead, the eukaryotic lipid cholesterol did to some extent counteract their penetration into the lipid films. Both temporin B and temporin L caused an enrichment of phospholipids in the bilayers, and in the presence of 1-palmitoyl-2-oleoyl-*sn*-glycero-3-phosphoglycerol (POPG), these peptides increased acyl chain order. Temporin B had practically no effect on giant liposomes composed of 1-stearoyl-2-oleoyl-*sn*-glycero-3-phosphocholine (SOPC), whereas rapid vesiculation was observed when POPG was present. In contrast, temporin L induced vesiculation of both SOPC and SOPC/POPG giant vesicles while the presence of cholesterol in SOPC giant vesicles attenuated this effect.

Antimicrobial peptides are widely distributed in nature, being a crucial component of the innate immunity of both invertebrates and vertebrates, which they protect against the invasion and proliferation of a wide array of noxious microorganisms. The skin of Anurans (frogs and toads), in particular, has been found to be a rich source of antimicrobial peptides displaying a large diversity both in their structure and in the spectrum of activity (*1, 2*). Often produced in large quantities, several different peptides with distinct antimicrobial specificities are generally present in the skin extract of a single animal. This diversity is believed to be important in protecting frogs from a wider range of harmful invaders (*3*). Frog skin antimicrobial peptides are produced and stored in specialized dermic structures called granular glands, which liberate their contents during adrenergic stimulation or as a result of skin lesions. A large and expanding group of frog antimicrobial peptides, collectively called prepro-dermaseptins, has been shown to have a highly conserved N-terminal preprosequence and a C-terminal domain with variable sequences corresponding to antimicrobial peptides (*4*).

Intense research focusing on antimicrobial peptides from frog skin as well as from other sources is currently devoted to elucidate their mechanisms of action. As an outcome of this work, antimicrobial peptides are generally believed to kill the target cell, either prokaryotic or eukaryotic, by permeabilizing or destabilizing the cell membrane. However, the precise mechanism(s) remain(s) incompletely understood. A number of excellent recent reviews on the interactions of antimicrobial peptides with biological and model membranes is available, offering a complete view of the different models proposed so far to account for the peptide-induced membrane permeation process (*5*−*8*).

Temporins are a family of antimicrobial peptides first isolated from the skin of the European red frog, *Rana temporaria* (*9*). Recently, new members of the temporin family have been found in extracts of the skin of other species of the genus *Rana*, viz., *R. clamitans* (*10*), *luteiventris* (*11*), *pipiens* (*11*), and *grylio* (*12*). These findings may thus provide insight also into the evolution and differentiation of these peptides among related species (*10, 11*). Temporins are linear 10−13 residue long peptides with a net positive charge and an amidated C-terminus, and they potentially assume an amphipathic α-helical conformation in apolar

[†] This study was supported by the Technology Development Fund (TEKES) and the Finnish Academy. A.C.R. was supported by a FEBS Short-Term Fellowship.

* Address correspondence to this author at the Helsinki Biophysics & Biomembrane Group, Institute of Biomedicine, University of Helsinki, P.O. Box 63 (Haartmaninkatu 8), FIN-00014, Finland. Tel: +358-9-19125400, Fax: +358-9-19125444, Email: Paavo.Kinnunen@Helsinki.Fi.

[‡] University of Helsinki.

[§] Università di Cagliari.

[||] Università dell'Aquila.

[⊥] Università "La Sapienza".

10.1021/bi011929e CCC: $22.00
Published on Web 03/06/2002

solvents such as trifluoroethanol (*9*, *13*). Temporins A and B were found to be active also against cell-wall-defective mutant strains of *E. coli* and release liposome-entrapped fluorescent probes (*9*, *13*). One member of this family, temporin D, has a lytic effect on erythrocytes (*13*). A recent investigation of the stability in the fecal milieu of two different enantiomers of temporin B showed that the D isomer of the peptide was inactivated more slowly than the L isomer (*14*). Accordingly, D isomers may thus be preferable when therapeutic use is considered.

The interactions of temporins with lipids have not been addressed in detail. To get more insight into the mode of action of these peptides and to compare them to magainin 2 and indolicidin, two other antimicrobial peptides which have been previously studied by our laboratory (*15*), we studied the interactions of temporin B (LLPIVGNLLKSLL-NH_2) and temporin L (FVQWFSKFLGRIL-NH_2) with model membranes. More specifically, we investigated their ability to insert into lipid monolayers, the effects on the structural dynamics of lipid bilayers using diphenylhexatriene (DPH)[1] and pyrene-labeled phospholipids, and the impact on the morphology of giant liposomes.

MATERIALS AND METHODS

Materials. Hepes and EDTA were from Sigma. 1-Stearoyl-2-oleoyl-*sn*-glycero-3-phosphocholine (SOPC), 1-palmitoyl-2-oleoyl-*sn*-glycero-3-phosphoglycerol (POPG), and β-cholesterol were from Avanti Polar Lipids (Alabaster, AL). The fluorescent phospholipid analogue 1-palmitoyl-2-[10-(pyren-1-yl)decanoyl]-*sn*-glycero-3-phosphocholine (PPDPC) was from K&V Bioware (Espoo, Finland) and diphenylhexatriene (DPH) from EGA Chemie (Steinheim, Germany). Concentrations of the nonlabeled lipids were determined gravimetrically with a high-precision electrobalance (Cahn, Cerritos, CA) and those of the pyrene containing phospholipid and DPH spectrophotometrically by absorbance at 341 nm, using molar extinction coefficients of 38 000 and 88 000 cm^{-1}, respectively. The purity of the lipids was checked by thin-layer chromatography on silicic acid coated plates (Merck, Darmstadt, Germany) developed with chloroform/methanol/water (65:25:4, v/v/v). Examination of the plates after iodine staining and, when appropriate, upon UV-illumination revealed no impurities. Synthetic temporins were purchased from Tana Laboratories (Houston, TX). The purity of the peptides (>90% and >94% for temporin B and temporin L, respectively) was analyzed by HPLC, and their sequences were verified by both automated Edman degradation and mass spectrometry. Peptide concentrations were determined gravimetrically and by quantitative ion-exchange column chromatography and ninhydrin derivatization.

[1] Abbreviations: DPH, diphenylhexatriene; I_e, excimer fluorescence intensity of pyrene at 480 nm; I_m, monomer fluorescence intensity of pyrene at 398 nm; HMC, Hoffman modulation contrast; LUVs, large unilamellar vesicles; POPG, 1-palmitoyl-2-oleoyl-*sn*-glycero-3-phosphoglycerol; PPDPC, 1-palmitoyl-2-[10-(pyren-1-yl)decanoyl]-*sn*-glycero-3-phosphocholine; *r*, anisotropy of diphenylhexatriene; RFI_m, relative fluorescence intensity of pyrene monomers; RFI_e, relative fluorescence intensity of pyrene excimers; $R(I_e/I_m)$, relative excimer-to-monomer ratio of PPDPC fluorescence; SOPC, 1-stearoyl-2-oleoyl-*sn*-glycero-3-phosphocholine; *X*, mole fraction of indicated lipid; π, surface pressure; π_0, initial surface pressure; $\Delta\pi$, change of surface pressure; $\Delta I_m/\Delta[M]$, slopes for the increase in I_m due to temporin B before reaching saturating responses in RFI_m.

Penetration of Peptides into Lipid Monolayers. Insertion of peptides into lipid monolayers residing on an air/water interface was measured using magnetically stirred circular Teflon wells (Multiwell plate, subphase volume 1.2 mL, Kibron Inc., Helsinki, Finland). Surface pressure (π) was monitored with a Wilhelmy wire attached to a microbalance (DeltaPi, Kibron Inc.) connected to a Pentium PC. The indicated lipids were spread onto the air/buffer (5 mM Hepes, 0.1 mM EDTA, pH 7.0) interface in chloroform (approximately 1 mg/mL). Subsequently, the lipid monolayers were allowed to settle for approximately 15 min at different initial surface pressures (π_0) before the injection of temporins (0.3 μM final concentration) into the subphase. The increment in π after the injection of peptides was complete within approximately 30 min, and the difference between the initial surface pressure (π_0) and the value observed after the penetration of peptides into the films was taken as $\Delta\pi$. The data are represented as $\Delta\pi$ vs π_0. These graphs also yield the critical surface pressure π_c corresponding to the lipid lateral packing density preventing the intercalation of the peptides into films. All measurements were made in triplicate and performed at ambient temperature ($\approx$+24 °C).

Preparation of Large Unilamellar Vesicles (LUVs). Appropriate amounts of the lipid stock solutions were mixed in chloroform to obtain the desired compositions with PPDPC ($X = 0.01$) or DPH ($X = 0.002$) included as fluorescent probes. The solvent was removed under a stream of nitrogen, and the lipid residue was subsequently maintained under reduced pressure for at least 2 h. The dry lipids were then hydrated at 50 °C in 5 mM Hepes, 0.1 mM EDTA, pH 7.0, to yield a lipid concentration of 1 mM. The resulting dispersions were extruded through a stack of two polycarbonate filters (100 nm pore-size, Bedford, MA) using a Liposofast low-pressure homogenizer (Avestin, Ottawa, Canada) to obtain large unilamellar vesicles, with average diameters between 111 and 117 nm (*17*).

Measurement of I_e/I_m. Irradiation of pyrene at $\approx$344 nm generates a monomeric excited state, which relaxes back to ground state by emitting photons with a maximum at $\approx$398 nm (I_m), the exact peak energy and spectral structure depending on solvent polarity. If the local concentration of pyrene is high enough, the excited monomer may collide with a ground-state pyrene, forming an excited dimer (excimer). The excimer dissociates back to two ground-state pyrenes by emitting quanta as a broad and featureless band centered at $\approx$480 nm (*18*, *19*). Fluorescence emission spectra for LUVs labeled with PPDPC ($X = 0.01$) were measured with a Perkin-Elmer LS50B spectrofluorometer with a magnetically stirred, thermostated cuvette compartment. Bandwidths of 4 nm were used for both excitation and emission. The lipid concentration used was 20 μM with temperature maintained at 25 °C. After addition of appropriate amounts of peptides, samples were equilibrated for 5 min before recording the spectra. Three scans were averaged, and the emission intensities at $\approx$398 and 480 nm were taken for I_m and I_e, respectively.

Fluorescence Anisotropy (r) of DPH. DPH was included in liposomes at $X = 0.002$. The lipid concentration used was 20 μM with the temperature maintained at 25 °C. Polarized emission was measured in the L-format using Polaroid film-type filters with Perkin-Elmer LS50B. Fluorescence anisotropy, *r*, for DPH was measured with excitation at 360 nm

and emission at 450 nm, using 10 nm bandwidths, and its values were calculated using routines of the software provided by Perkin-Elmer.

Formation of Giant Liposomes. Giant liposomes were prepared as described elsewhere (*20*−*22*). Approximately 1−3 μL of the indicated lipids dissolved in diethyl ether/methanol (9:1, v/v, at a concentration of 1 mM) was spread onto the surface of the two Pt electrodes and subsequently dried under a stream of nitrogen. Possible residues of the organic solvents were removed by evacuation in a vacuum for 1 h. A glass chamber with the attached electrodes and a quartz window bottom was placed on the stage of a Zeiss IM-35 inverted fluorescence microscope. An AC field (sinusoidal wave function with a frequency of 4 Hz and amplitude of 0.2 V) was applied before adding 1.3 mL of 0.5 mM Hepes buffer, pH 7.4. During the first minute of hydration, the voltage was increased to 1.0 V. The AC field was turned off after 2 h, and giant liposomes were observed with Hoffman modulation contrast (HMC) optics with a 10×/0.25 objective (Modulation Optics Inc., New York). The size of giant liposomes was measured using calibration of the images by motions of the micropipet as proper multiples of the step length (50 nm) of the micromanipulator (MX831 with MC2000 controller, SD Instruments, Grants Pass, OR). Images were recorded with a Peltier-cooled 12-bit digital CCD camera (C4742-95, Hamamatsu, Japan) interfaced to a computer, and operated by the software (HiPic 5.0.1) provided by the camera manufacturer.

Microinjection Techniques. Micropipets with inner tip dimeters of >0.5 μm (*23*) were made from borosilicate capillaries (1.2 mm outer diameter) by a microprocessor-controlled horizontal puller (P-87, Sutter Instrument Co., Novato, CA). Indicated amounts of the peptide solutions (0.5 mM in 10 mM Hepes, 0.1 mM EDTA, pH 7.0) were applied onto the outer surface of individual giant liposomes as a series of single injections of approximately 20 fL delivered with a pneumatic microinjector (PLI-100, Medical Systems Corp., Greenvale, NY). For easier handling, only vesicles attached to the electrode surface were used. All experiments were performed at ambient temperature (≈+24 °C) and repeated at least 10 times.

RESULTS

Penetration of Temporins into Lipid Monolayers. Insertion of ligands such as peptides into lipid monolayers on an air/water interface following their injection in the aqueous subphase causes an increase $\Delta\pi$, in surface pressure. The data obtained are represented as $\Delta\pi$, as a function of the initial surface pressure of the film, π_0 (*15*, *16*). The magnitude of the surface pressure change can be used to assess the relative energies of peptide−lipid interactions and characterize lipid specificity of peptides (for a review, see *16*). Previous studies employing this technique have revealed antimicrobial peptides such as magainin 2 and indolicidin to efficiently intercalate into lipid films (*15*). Likewise, both temporin B and temporin L intercalated effectively into lipid monolayers, as shown for a SOPC/POPG film ($X_{POPG} = 0.20$) at an initial pressure (π_0) of ≈15 mN/m (Figure 1). Yet, the kinetics of the increase in surface pressure for the two peptides were distinctly different. Accordingly, after the addition of temporin B into the subphase (Figure 1, panel A), there was a fast transient peak in π, followed first by a relaxation and subsequently by a slow increase in π. These kinetics were independent from lipid composition, and initial surface pressure varied in the range of 12−36 mN/m. In contrast, for temporin L, the value for surface pressure increased in a continuous manner, reaching a plateau within approximately 40 min (Figure 1, panel B). The kinetics were not investigated in more detail at this stage.

Data from similar measurements as above were subsequently analyzed in terms of $\Delta\pi$ vs π_0 (Figure 1, panels C and D). Temporin B readily inserted into SOPC monolayers up to $\pi_0 \approx 39$ mN/m, where the slope for the $\Delta\pi-\pi_0$ data points extrapolates to $\Delta\pi = 0$. This value thus represents the critical packing pressure π_c above which this peptide no longer intercalates into the SOPC monolayer (Figure 1, panel C). In keeping with its net positive charge of +2, the penetration of temporin B into lipid monolayers was progressively augmented when the content of the acidic phospholipid POPG in the films was increased (Figure 1, panel C), the value for π_c increasing dramatically. Interestingly, upon varying X_{POPG} between 0.10 and 0.40, the $\Delta\pi$ vs π_0 data for temporin B exhibit a 'crossover' point at a surface pressure of ≈32 mN/m. Specifically, below the latter surface pressure, the increment in $\Delta\pi$ was augmented with increasing POPG in the film whereas the opposite was observed at $\pi_0 > 32$ mN/m. The values for π_c decreased in the sequence ≈64, ≈55, and ≈48 mN/m upon increasing X_{POPG} from 0.10 to 0.20 and 0.40, respectively (Figure 1, panel E). The inclusion of cholesterol ($X = 0.10$) into the SOPC film suppressed the insertion of this peptide into the monolayer at $\pi_0 <$ ≈27 mN/m (Figure 1, panel C), while π_c increased to ≈42 mN/m.

A pronounced increase in π was observed also due to temporin L, revealing its penetration into the SOPC monolayers (Figure 1, panel D). However, temporin L is significantly more membrane-active than temporin B, with $\pi_c \approx$ 54 mN/m. Analogously to temporin B, the presence of increasing contents of POPG in the monolayer enhanced the penetration of temporin L, increasing $\Delta\pi$ below ≈43 mN/m (Figure 1, panel D). However, above the latter 'crossover' value for surface pressure, the increment in π due to temporin L was slightly attenuated by POPG, causing decrement in π_c in the presence of POPG, shifting to ≈53, ≈51, and ≈50 mN/m at $X_{POPG} = 0.10$, 0.20, and 0.40, respectively (Figure 1, panel E). As for temporin B, the increment in π due to temporin L was attenuated by cholesterol ($X_{chol} = 0.10$), while π_c decreased from ≈54 to ≈48 mN/m (Figure 1, panel D).

Effects of Temporins on the Lipid Dynamics in Bilayers. Consequences of the association of the peptides with liposomes were subsequently studied by recording the emission spectra for the pyrene-labeled fluorescent phospholipid analogue PPDPC ($X = 0.01$) incorporated into LUVs. For a single pyrene moiety containing a lipid analogue such as PPDPC, steady-state I_e/I_m values reflect the lateral mobility as well as the local concentration of the fluorophore in the membrane (*18*, *19*). Yet, our previous studies comparing the effects on membrane lipid dynamics by two other antimicrobial peptides, magainin 2 and indolicidin, revealed that these peptides also influence the quantum yields of pyrene-labeled lipids (*15*). For SOPC LUVs, the addition of temporin B caused a significant decrease in *both* pyrene

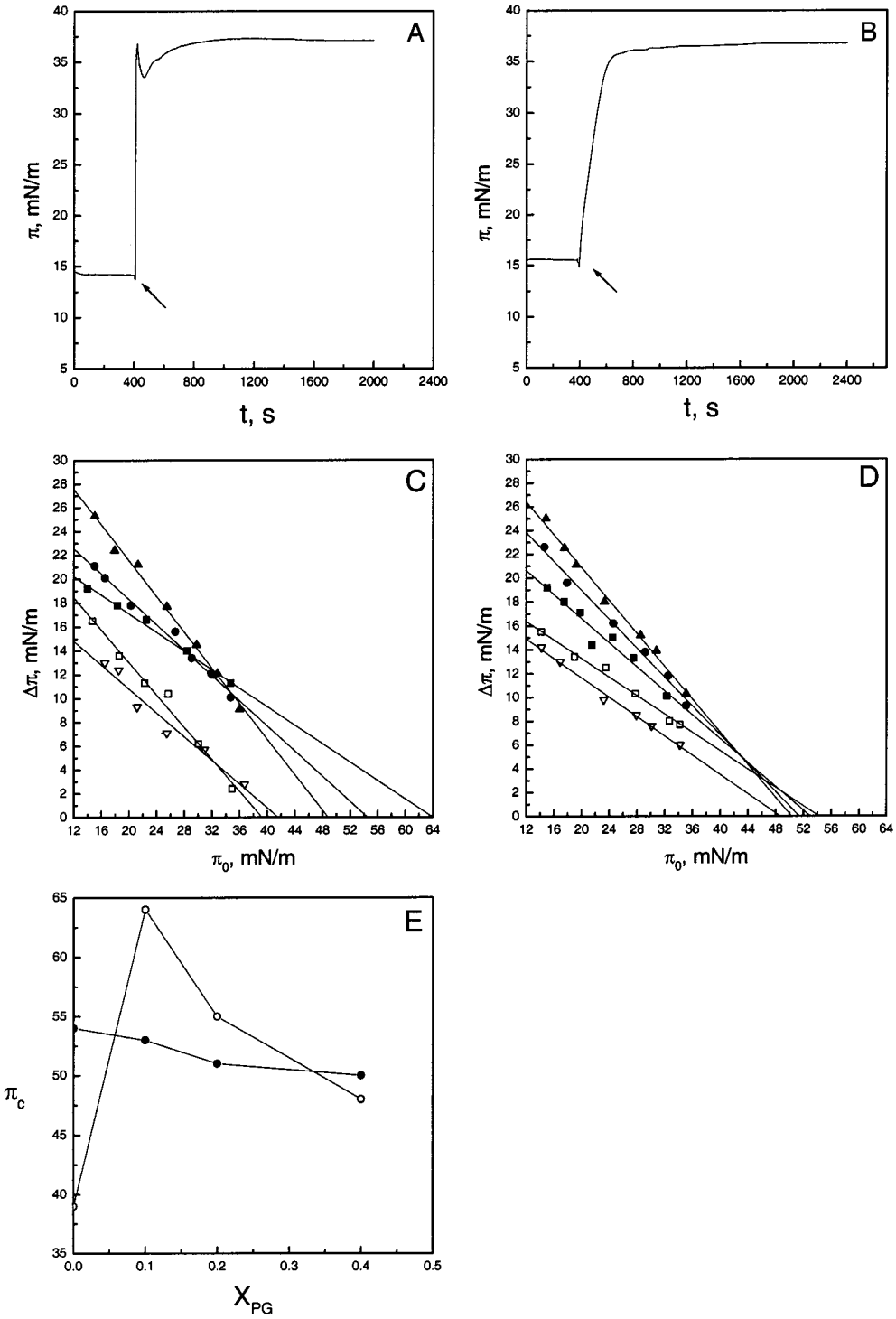

FIGURE 1: Insertion of temporins B and L into lipid monolayers. Increase in surface pressure as a function of time following the injection of either temporin B (panel A) or temporin L (panel B) underneath a SOPC/POPG ($X_{POPG} = 0.2$) monolayer at the initial surface pressures (π_0) of 14.6 and 15.5 mN/m, respectively. The additions of the peptides (0.3 μM final concentration) are marked by arrows. Increments in surface pressure ($\Delta\pi$) of lipid monolayers due to the addition of 0.3 μM temporin B (panel C) or temporin L (panel D) into the subphase are illustrated as a function of the initial surface pressure (π_0). Contents of POPG (X_{POPG}) in SOPC were 0 (□), 0.10 (■), 0.20 (●), and 0.40 (▲). Also shown is the insertion of the peptides into a SOPC film with $X_{chol} = 0.1$ (▽). Panel E shows the values for π_c as a function of X_{POPG} upon the penetration of temporin B (○) and temporin L (●), respectively. Each data point represents the mean of triplicate measurements. The standard deviation varied between 0.1 and 0.8 mN/m and for the sake of clarity is not shown.

monomer and excimer emission, I_m and I_e, respectively, with a maximum decrement by approximately 40% (Figure 2, panels A and B). The quenching of pyrene fluorescence bands was biphasic, with a pronounced decrease in the quantum yield at a temporin B:lipid molar ratio of approximately 1:12 (Figure 2, panels A and B). Quenching of pyrene monomer and excimer fluorescence by temporin B was evident also in the presence of cholesterol ($X_{chol} = 0.10$) although the decrement in emission was less than that observed for SOPC LUVs (Figure 2, panels A and B). However, when the acidic phospholipid POPG was present at $X_{POPG} = 0.10$, only insignificant changes in I_m were evident, and upon increasing X_{POPG} from 0.20 to 0.40, temporin B caused I_m to increase in a progressive manner

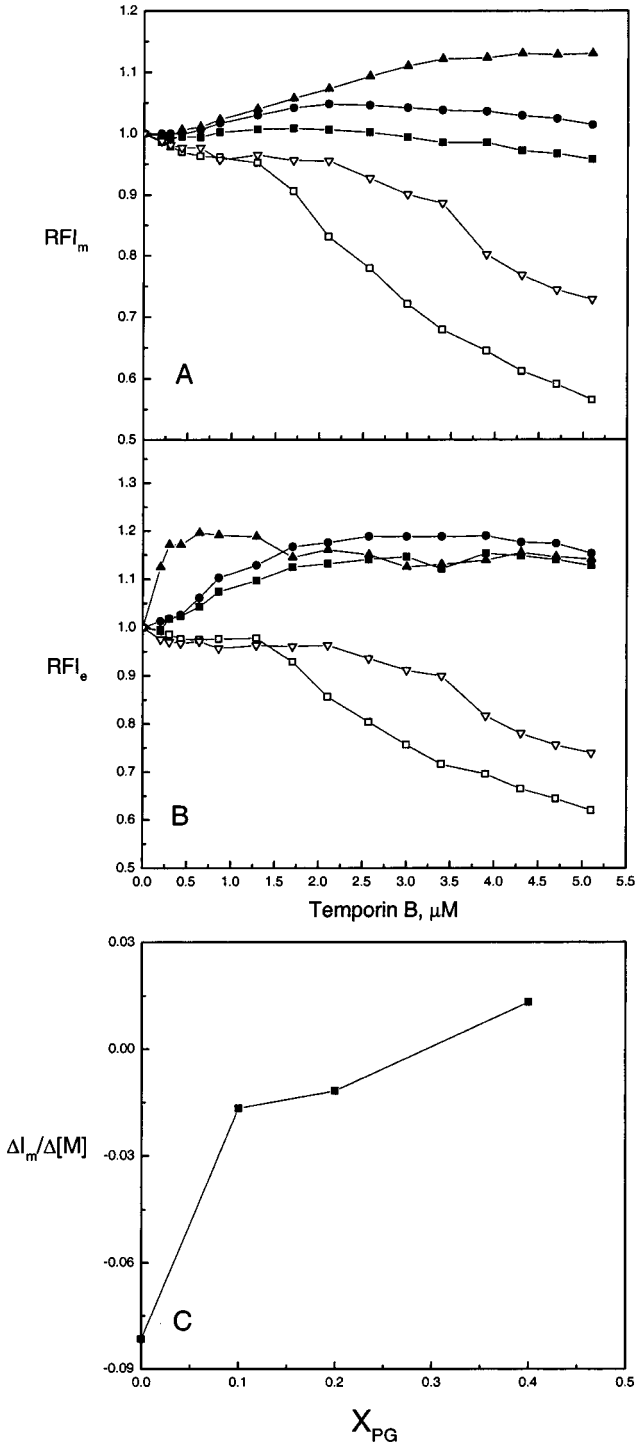

FIGURE 2: Effects of temporin B on lipid dynamics in LUVs assessed by the fluorescence of the pyrene-labeled phospholipid PPDPC ($X = 0.01$), shown as changes in pyrene monomer and excimer emission intensity I_m (panel A), I_e (panel B), and slopes for the increase in I_m before reaching saturating responses in RFI$_m$ (panel C), respectively. Liposomes were composed of SOPC with $X_{POPG} = 0$ (□), 0.10 (■), 0.20 (●), and 0.40 (▲), and with $X_{chol} = 0.10$ (▽). The concentration of lipids was 20 μM in a total volume of 2 mL of 5 mM Hepes, 0.1 mM EDTA, pH 7.0. The temperature was maintained at 25 °C with a circulating waterbath. Each data point represents the mean of triplicate measurements. The standard deviation is less than 0.02 (panels A and B) and 0.004 (panel C), and for the sake of clarity is not shown.

with the initial increment in I_m leveling off at a POPG/temporin B stoichiometry of approximately 2/1. The slopes of the linear increments in I_m before reaching saturating

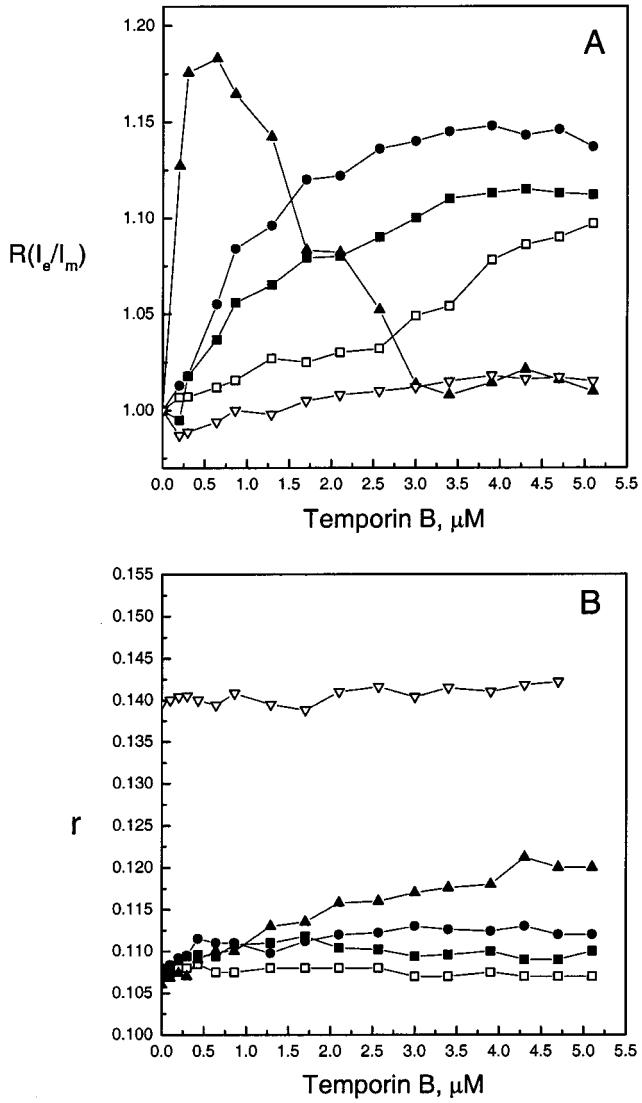

FIGURE 3: Effects of temporin B on lipid dynamics in LUVs assessed by fluorescence of the pyrene-labeled phospholipid PPDPC ($X = 0.01$) and the steady-state emission anisotropy r of DPH ($X = 0.002$), shown as changes in the normalized excimer to monomer ratio $R(I_e/I_m)$ (panel A) and anisotropy r (panel B) in SOPC liposomes with $X_{POPG} = 0$ (□), 0.10 (■), 0.20 (●), and 0.40 (▲), and with $X_{chol} = 0.10$ (▽). Each data point represents the mean of triplicate measurements. The standard deviation is less than 0.02 (panel A) and 0.004 (panel B), and for the sake of clarity is not shown. Otherwise conditions were as described in the legend for Figure 2.

responses increased with X_{POPG} (Figure 2, panel C). In the presence of POPG, also I_e was increased by temporin B. At $X_{POPG} = 0.40$, the values for I_e increased progressively up to a temporin B:lipid molar ratio of ≈1:15, corresponding to a peptide/POPG stoichiometry of ≈1/6, whereas upon exceeding this stoichiometry I_e decreased. Changes in I_e/I_m due to temporin B are shown in Figure 3, panel A. Specifically, I_e/I_m was increased for SOPC LUVs maximally 1.1-fold while only minor changes in I_e/I_m were observed in the presence of cholesterol ($X_{chol} = 0.10$, Figure 3, panel A). Increasing X_{POPG} from 0.10 to 0.20 progressively enhanced the increment in I_e/I_m. Interestingly, at $X_{POPG} = 0.40$, the increment in I_e/I_m was evident at a temporin B:lipid molar ratio of ≈1:30. However, above this peptide:lipid ratio, temporin B caused I_e/I_m to decrease, and insignificant changes

in I_e/I_m were evident above a peptide:lipid ratio of ≈1:6.

The augmented I_e/I_m for the pyrene-labeled lipid PPDPC is in general assessed to result either from lateral segregation of the probe or from an increased rate of lipid lateral diffusion. To resolve between these two mutually nonexclusive mechanisms, we measured the steady-state fluorescence anisotropy *r* for DPH in the membrane (Figure 3, panel B). DPH is a small, hydrophobic and rod-like fluorophore, a large fraction of which resides in the hydrocarbon region of bilayers, oriented parallel to the long axis of membrane lipids. Its emission anisotropy can be used to assess acyl chain order (for a review, see *24*). Increasing acyl chain order is observed upon augmented packing of lipids, thus diminishing lipid lateral diffusion (*25*, *26*). Temporin B caused only insignificant changes in *r* for both SOPC and SOPC/cholesterol (X_{chol} = 0.10) LUVs (Figure 3, panel B). Accordingly, lack of changes in acyl chain order for SOPC LUVs together with the increase in I_e/I_m reveals that an enrichment of PPDPC into microdomains is likely to take place. Progressively enhanced lipid packing and acyl chain order upon the addition of temporin B were evident with increasing X_{POPG}. An increase in membrane lateral diffusion thus cannot be causing the observed increase in I_e/I_m and temporin B-induced segregation of lipids; viz., clustering of PPDPC in the membrane can be concluded. However, the interpretation becomes more complicated when the impact of the quenching processes is taken into account.

Subsequently, we carried out identical measurements as described above but using temporin L. Both I_e and I_m decreased upon the addition of temporin L into SOPC LUVs (Figure 4, panels A and B), with their decrement leveling off at a peptide:lipid molar ratio ≈ 1:8. The decrease in I_e and I_m was somewhat smaller when cholesterol (X_{chol} = 0.10) was included in SOPC LUVs, yet again leveling off at a temporin L/lipid stoichiometry of ≈1/8. Very different effects of the peptide were seen when the acidic phospholipid POPG was present. In contrast to temporin B, temporin L decreased I_m for LUVs containing the acidic phospholipid POPG, with the largest effect at X_{POPG} = 0.10 (Figure 4, panel A). Interestingly, at X_{POPG} = 0.10, a clear discontinuity is evident, corresponding to POPG:temporin L molar ratio of 1:1 and thus suggesting stoichiometric complex formation. The decrement in I_m leveled off at a temporin L:lipid molar ratio ≈1:5 at X_{POPG} = 0.10 while continuous decrement was evident at X_{POPG} = 0.20 and 0.40 (Figure 4, panel A). The decrement in I_m was progressively attenuated with increasing contents of POPG in the liposomes. At X_{POPG} = 0.10, the values for I_e decreased less than for SOPC LUVs when the temporin L:lipid molar ratio was ≤≈1:8. Exceeding this stoichiometry, the largest decrement in I_e was evident at X_{POPG} = 0.10, and the decrement reached a plateau at a temporin L:lipid molar ratio ≈1:5 (Figure 4, panel B). Similarly to I_m, the decrement in I_e due to temporin L was progressively attenuated with increasing X_{POPG}. The effects on I_e/I_m by temporin L are depicted in Figure 5, panel A. A slight increase in I_e/I_m for SOPC LUVs was evident upon the addition of temporin L (Figure 5, panel A), whereas a significant increase was observed in the presence of POPG. Interestingly, minor difference of the increment in I_e/I_m due to temporin L was evident at X_{POPG} = 0.10, 0.20, and 0.40 below a temporin L:lipid molar ratio of ≈1:10. However, above a temporin L/lipid stoichiometry of ≈1/8, the increments in I_e/I_m at X_{POPG} = 0.20 and 0.40 were significantly higher than those at X_{POPG} = 0.10. Likewise, I_e/I_m increased further at X_{POPG} = 0.40 above a temporin L/lipid stoichiometry of ≈1/6 (Figure 5, panel A).

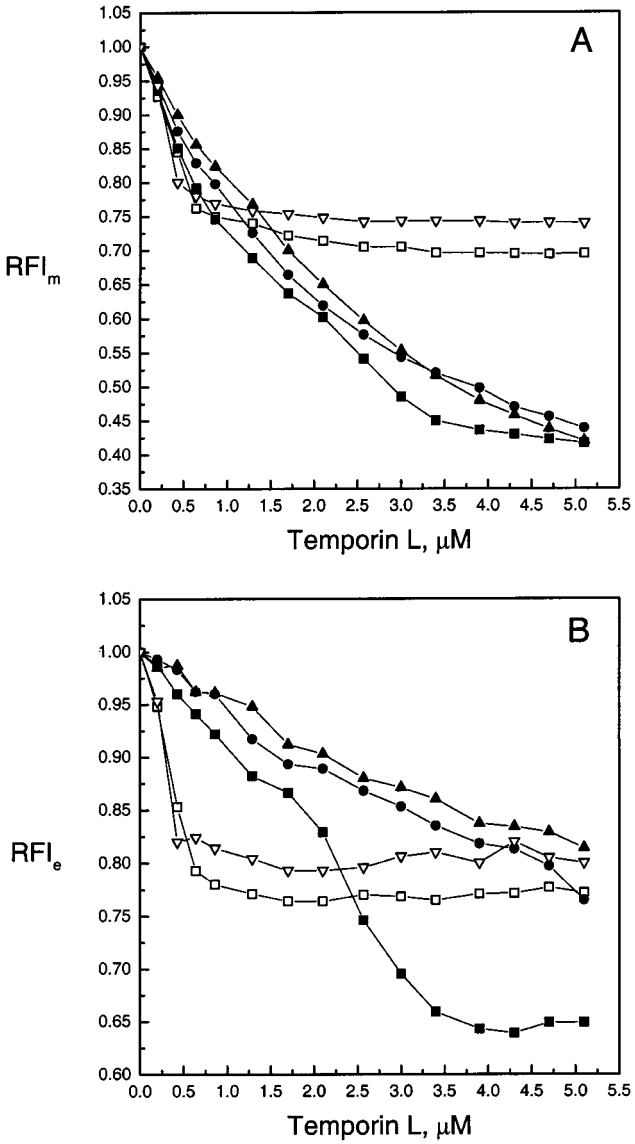

FIGURE 4: Effects of temporin L on lipid dynamics in LUVs assessed by the fluorescence of the pyrene-labeled phospholipid PPDPC (X = 0.01), shown as changes in pyrene monomer and excimer emission intensity I_m (panel A) and I_e (panel B), respectively. Liposomes were composed of SOPC with X_{POPG} = 0 (□), 0.10 (■), 0.20 (●), and 0.40 (▲), and with X_{chol} = 0.10 (▽). Each data point represents the mean of triplicate measurements. The standard deviation is less than 0.02 and for the sake of clarity is not shown. Otherwise conditions were as described in the legend for Figure 2.

For the same purpose as described above for temporin B, we measured also the changes in DPH anisotropy, *r*, induced by temporin L. Similarly to temporin B, only a minor change in *r* was evident when temporin L was added to SOPC and SOPC/cholesterol (X_{chol} = 0.10) LUVs (Figure 5, panel B). However, strongly augmented acyl chain order were caused by temporin L in the acidic phospholipid containing membranes, evident as a significant increase in DPH anisotropy (Figure 5, panel B). The increments in *r* were progressively increased with increasing X_{POPG} in the membranes above a temporin L:lipid molar ratio of ≈1:6. As temporin L caused

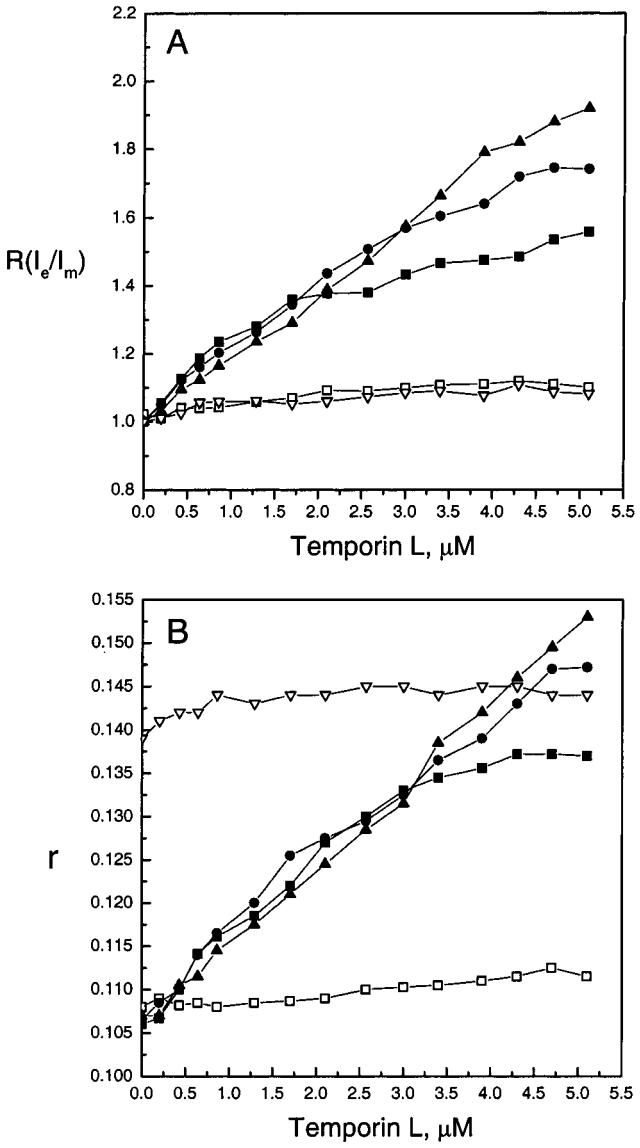

FIGURE 5: Effects of temporin L on lipid dynamics in LUVs assessed by the fluorescence of the pyrene-labeled phospholipid PPDPC ($X = 0.01$) and the steady-state emission anisotropy r of DPH ($X = 0.002$), shown as changes in the normalized excimer to monomer ratio R (I_e/I_m) (panel A) and anisotropy r (panel B) in SOPC liposomes with $X_{POPG} = 0$ (□), 0.10 (■), 0.20 (●), and 0.40 (▲), and with $X_{chol} = 0.10$ (▽). Each data point represents the mean of triplicate measurements. The standard deviation is less than 0.02 (panel A) and 0.004 (panel B), and for the sake of clarity is not shown. Otherwise conditions were as described in the legend for Figure 2.

a pronounced increase in I_e/I_m for SOPC and acidic phospholipid containing membranes, the enrichment of the fluorescent lipid PPDPC in these membranes is taking place.

Effects of Temporins on Membrane Topology. Giant liposomes represent an excellent model of biomembranes due to their large sizes comparable to cells. Moreover, they are amenable for observation by optical microscopy (*15*, *21*). Our previous studies on magainin 2 and indolicidin demonstrated these peptides have pronounced effects on the topology of giant liposome membranes (*15*). In this study, the effects of temporins on the 3-D topology of giant liposomes were observed under similar conditions by microscopy following the addition of these peptides on the outer surface of giant vesicles. SOPC giant liposomes were unaffected by temporin B even when exposed to high amounts of this peptide, approximately 1.2 fmol of temporin B (repeated 100 aliquots of 12 amol each). Likewise, also giant vesicles containing cholesterol ($X_{chol} = 0.10$) were unaffected by this quantity of temporin B. Yet, an adhesion between neighboring vesicles was occasionally observed upon the addition of this peptide onto the surface of SOPC and SOPC/cholesterol ($X_{chol} = 0.10$) giant liposomes (data not shown). However, in the presence of POPG ($X_{POPG} = 0.10$), already ≈36 amol (10^{-18} M) of temporin B (approximately 60 fL, 3 injections) applied onto the surface of the giant vesicle induced significant changes in the topology of the giant vesicle membrane (Figure 6, panel B). Specifically, small particles ($\phi \approx 10$ μm) emerged on the surface of the membrane and subsequently moved into the internal cavity of the giant liposome (Figure 6, panel B). Further addition of ≈0.24 fmol of temporin B (approximately 400 fL, 20 injections) caused the number of these particles inside the giant vesicle (Figure 6, panel C) to increase. Aggregation of particles on the surface of the giant vesicle was also observed (Figure 6, panel C). Subsequently, within ≈10 min, the particles transferred into the internal cavity of the giant liposome.

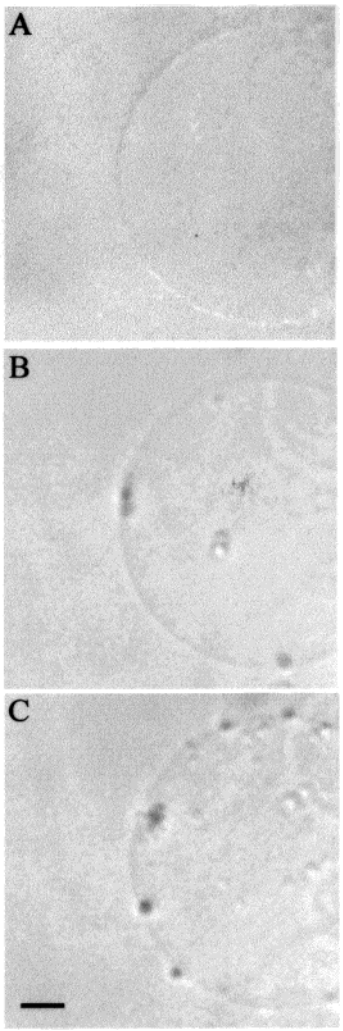

FIGURE 6: HMC images of the transformation of a giant SOPC/POPG ($X_{POPG} = 0.1$) liposome induced by temporin B. Giant vesicles prior to the addition of temporin B (panel A), 5 s after the application of ≈36 amol of temporin B (panel B), and after the addition of ≈0.24 fmol of temporin B (panel C). The length of the scale bar in panel C corresponds to 50 μm.

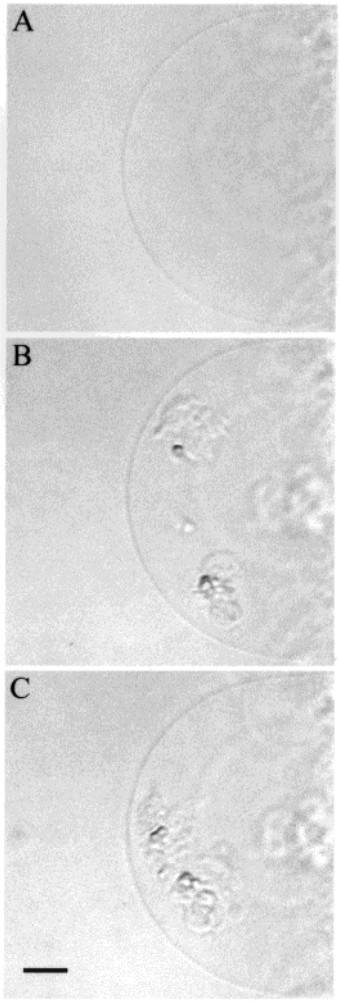

FIGURE 7: HMC images of the transformation of a SOPC giant liposome due to temporin L. Giant vesicles before the addition of temporin L (panel A), 1 s after the addition of ≈12 amol of temporin L (panel B), and 5 min after the application of a total of ≈0.12 fmol of temporin L (panel C). The length of the scale bar in panel C corresponds to 50 μm.

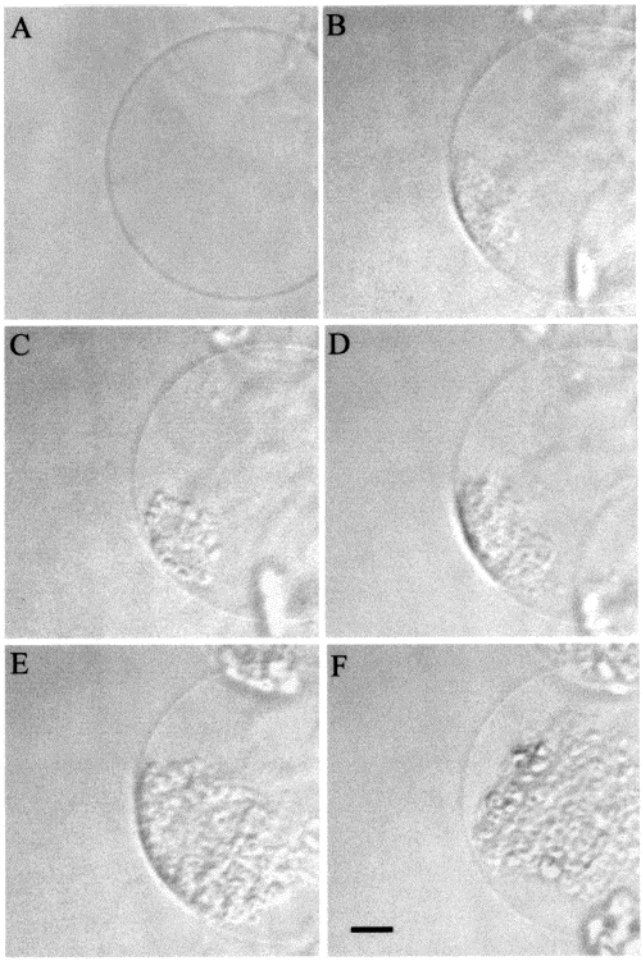

FIGURE 8: HMC images depicting the transformation of a giant SOPC/POPG ($X_{POPG} = 0.1$) liposome induced by temporin L. Giant vesicles before the application of temporin L (panel A), as well as immediately (panel B), 1 s (panel C) after the addition of ≈12 amol of temporin L, and immediately (panel D) after the addition of ≈24 amol of temporin L. Images were taken also immediately after the injection of a total of ≈36 amol (panel E) of temporin L, and 5 min (panel F) after the addition of a total of ≈60 amol of temporin L. The length of the scale bar in panel F corresponds to 50 μm.

We then studied the effects of temporin L on giant liposomes. The sequence of images shown in Figure 7 illustrates the transformation of a SOPC giant liposome due to temporin L. Interestingly, already approximately 12 amol of temporin L (1 injection) affected the appearance of the SOPC membrane, with aggregated structures emerging inside the giant vesicle within 1 s after the addition of the peptide (Figure 7, panel B). Also the neighboring giant vesicle was affected by similar vesiculation (Figure 7, panel B, underneath the giant liposome studied). Further addition of temporin L (up to ≈0.12 fmol, 10 repeated injections in total) induced no further vesiculation, while the two 'endocytotic' aggregates adhered to the giant liposome surface at the site of the microinjection of the peptide. After approximately 5 min, these two 'endocytotic' aggregates adhered, and a larger aggregated structure was formed inside the giant vesicle (Figure 7, panel C). Similarly to the effects of temporin L on SOPC giant liposomes, this peptide induced an endocytosis-like process in the presence of POPG ($X_{POPG} = 0.10$, Figure 8). More specifically, upon the addition of approximately 12 amol of temporin L (1 injection), the area of the giant liposome surface exposed to the peptide became dark, revealing a pronounced change in the refractive index and indicating the formation of a tightly packed 3-D structure, remaining only partly in the focal plane (Figure 8, panel B). Within ≈1 s, an aggregate of small particles appeared inside the giant liposome together with the dark domain (Figure 8, panel C). Simultaneously, vesiculation in the neighboring giant vesicles was also observed (Figure 8, panels B and C). Subsequent addition of a total of ≈24 amol of temporin L (2 injections) caused another 'endocytotic' group of small particles to emerge inside the giant liposome, adhering with the previously formed aggregate (Figure 8, panel D). After ≈1 min, some of these particles ($\phi \approx 8$ μm) were released from the bilayer inside the giant liposome (data not shown). Interestingly, upon further addition of approximately 12 amol of temporin L (3 injections in total), the separated small particles aggregated again, and the area of the dark domain increased (Figure 8, panel E). The increment in the area of the dark domain was augmented by the addition of a further ≈24 amol of temporin L (5 injections in total). After a few minutes, the aggregated 'endocytotic' small particles moved into the internal cavity of the giant vesicle, while the dark domain on the membrane surface disappeared (Figure 8, panel F). Concomitant vesiculation of the neighboring giant

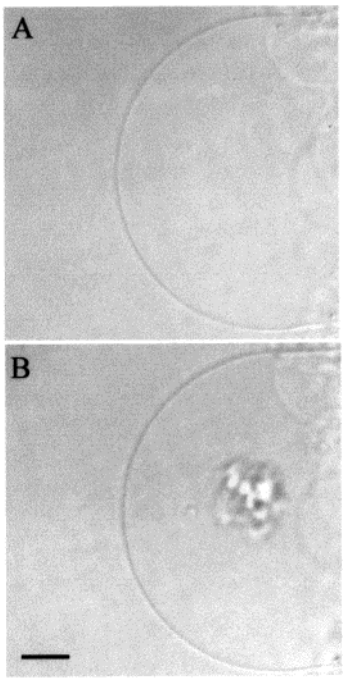

FIGURE 9: Sequence of HMC images illustrating the transformation of a SOPC/cholesterol ($X_{chol} = 0.10$) giant liposome by temporin L. Giant vesicle prior to the addition of the peptide (panel A) and immediately after the application of ≈0.24 fmol of temporin L (panel B). The length of the scale bar in panel B corresponds to 50 μm.

liposomes was also observed. Interestingly, in the presence of cholesterol ($X_{chol} = 0.10$), more temporin L was needed to induce vesiculation (Figure 9). Yet, after the addition of approximately 0.24 fmol (20 injections) of temporin L, an 'endocytotic' aggregate of small particles as well as a ≈9 μm diameter particle appeared inside the giant liposome (Figure 9, panel B). Subsequent addition of ≈0.24 fmol of the peptide (40 injections in total) induced another group of small particles inside the giant vesicle, which merged with the first aggregate after approximately 30 s (data not shown). However, subsequent further addition of temporin L (up to approximately 1.2 fmol, 100 injections) caused no further visible changes on the giant liposome membrane.

DISCUSSION

The long term aim of our effort is to establish minimal sequence requirements, which could be further used as guidelines in the design of novel antimicrobial peptidomimetics. We have previously compared the impact of two antimicrobial peptides, magainin 2 and indolicidin, on the same model membrane systems as used in this study, viz., monolayers, liposomes, and giant vesicles (*15*). The peptides employed in our earlier investigation were chosen as they represent two different types of antimicrobial peptide families. In the present study, we used two 13-amino acid peptides, i.e., of similar length as indolicidin. The peptides differ in structural parameters such as charge, conformation, hydrophobicity, hydrophobic moment, and size (Table 1). Interestingly, of the four peptides investigated, calculated on a molar basis temporin L is most effective and acts on both neutral as well as acidic phospholipid containing membranes. Its net cationic charges as well as hydrophobicity have average values when compared to the other three peptides (Table 1). However, of the peptides shown, temporin L has the highest mean hydrophobic moment, suggesting that this may be an important parameter correlating to its efficient membrane-perturbing action, in accordance with a previous study comparing magainin 2 and other antimicrobial peptides (*31*).

Although there are distinct differences in the effects of the above antimicrobial peptides on model biomembranes, also several similarities were evident. The interactions of all four peptides with lipids can be characterized in terms of different processes, as follows. The peptides first bind to and insert into the membranes. This process is enhanced by and involves the formation of a complex with acidic phospholipids. The insertion is accompanied by increment in acyl chain order. Due to the threshold peptide:lipid molar ratios, the overall interaction is cooperative and implies the formation of aggregated structures composed of peptide−acidic phospholipid complexes. Finally, there is also formation of more macroscopic aggregates, evident in the microscopy images. In the following, we will discuss the above process together with possible underlying mechanisms providing the respective driving forces.

Similarly to magainin 2 and indolicidin (*15*), both temporins B and L are highly membrane-active (Figure 1). Likewise, the interaction of all four peptides with monolayers was augmented in the presence of the acidic phospholipid, in keeping with their net positive charge (Table 1). CD spectra show that in a hydrophobic environment temporins adopt an α-helical structure (*13*, Zhao and Kinnunen, unpublished data). In addition, their helical-wheel projections reveal an amphiphilic nature. The kinetics of the increase in π caused by temporin B were different from those for temporin L (Figure 1, panels A and B) and suggest a conformational and/or orientational change following the initial intercalation of the former peptide into the lipid film. In other words, the interaction of temporin B with lipid monolayers would consist of the following steps, viz.: (i) binding of temporin B to the monolayer surface, (ii) intercalation of temporin B into the lipid films, probably with its long axis parallel to the membrane layer plane, and (iii) rapid reorientation of the peptide, perpendicular to the

Table 1: Comparison of the Mean Residue Hydrophobicities (H) and Hydrophobic Moments (μ) of the Antimicrobial Peptides[a]

peptide	sequence	number of residues	H	μ	conformation in lipid membranes	net charge at physiological pH
magainin 2	GIGKFLHSAKKFGKAFVGEIMNS	23	−0.0356	0.286	α-helix [b]	+4
indolicidin	ILPWKWPWWPWRR-NH_2	13	−0.1385	0.195	non-α-helix [c]	+4
temporin b	LLPIVGNLLKSLL-NH_2	13	0.1954	0.307	α-helix [d]	+2
temporin l	FVQWFSKFLGRIL-NH_2	13	0.06461	0.312	α-helix [e]	+3

[a] Mean residue hydrophobicities and hydrophobic moments per residue were calculated using the Eisenberg consensus scale of hydrophobicity (*27*). [b] See ref (*28*). [c] See refs (*29, 30*). [d] See ref (*13*). [e] Zhao and Kinnunen, unpublished work.

monolayer surface. The latter process would thus cause the observed abrupt decrease in π (Figure 1, panel B). Yet, it is also possible that during (iii) some POPG molecules associated with the peptide become oriented differently from phospholipids of the bulk of the monolayer, as suggested for indolicidin (*15*).

The presence of POPG caused augmented $\Delta\pi$ due to temporin B at $\pi < 32$ mN/m, the latter value thus representing a 'crossover' point in the $\Delta\pi-\pi_0$ graphs, similarly to indolicidin (*15*). Accordingly, below the latter surface pressure, $\Delta\pi$ was progressively increased with increasing X_{POPG} whereas the opposite was observed at $\pi > 32$ mN/m. A similar 'crossover' point although at a higher surface pressure of ≈43 mN/m is also evident for temporin L (Figure 1, panels D and E). However, for this peptide, a decrease in π_c with increasing X_{POPG} was evident (Figure 1, panel E). A 'crossover' point at ≈38 mN/m was observed for indolicidin in our previous study. Interestingly, however, this characteristic was absent for magainin 2 (*15*). The possible significance of the 'crossover' point to the mechanism(s) of action of these peptides warrants further studies. For eukaryote plasma membranes, the equilibrium lateral pressure has been estimated at ≈32 mN/m (for brief reviews, see *16, 32*). As far as we know, the equilibrium lateral pressure of prokaryote membranes is not known. Yet, it seems reasonable to assume that basic physicochemical properties of the bilayer could dictate the lateral pressures in the two types of cells to be of similar magnitude. Qualitatively, it is of interest that the more surface-active peptides, temporin L and indolicidin, have high values of 'crossover' pressures.

Effects of temporin B and temporin L on lipid dynamics in the bilayers reported here were strikingly similar to those reported previously for magainin 2 and indolicidin (*15*). Accordingly, the increment in DPH anisotropy *r* revealed that all these peptides increased acyl chain order in the presence of the acidic phospholipid POPG, the magnitude of this effect increasing with X_{POPG}. Likewise, lipid segregation was induced in the presence of the acidic phospholipid. All these effects imply the importance of the acidic phospholipid as well as the cationic charge of the peptides for the interaction of the latter with biomembranes. For magainin 2 and temporin B, quenching of pyrene fluorescence in SOPC and SOPC/cholesterol ($X_{chol} = 0.10$) liposomes was abolished in the presence of POPG while for temporin L and indolicidin this process was observed regardless of lipid composition. Both $\pi-\pi$ interactions between pyrene and Trp as well as contacts of the basic residues of the peptides (*15*) with the fluorophore resulting in $\pi-$cation interaction (*33*) may be involved in the quenching. In addition, the microenvironment of the fluorophore could become more hydrophilic in the presence of the peptides, thus reducing the fluorescence quantum yield. In contrast to magainin 2 and indolicidin (*15*), quenching of pyrene due to temporins B and L was attenuated in the presence of cholesterol ($X_{chol} = 0.10$), thus suggesting that cholesterol may counteract the membrane insertion of the latter two peptides.

At $X_{POPG} = 0.40$, temporin B induced a maximum increase in I_e/I_m at a peptide:lipid molar ratio of ≈1:30 whereas above this stoichiometry I_e/I_m decreased (Figure 3, panel A). Due to the strong interaction of temporin B with the membrane at $X_{POPG} = 0.40$, different effects may contribute to the reduction of the excimer formation of pyrene lipid analogue, as follows. First, the membrane-bound temporin B could represent a mechanical barrier for the lateral diffusion of the fluorescent probe. In other words, the membrane-associated peptides could statically reduce excimer formation by occupying neighboring positions of the probe and thus increase the path length for the diffusion of the pyrene-labeled lipid between collisions. Second, the rotational freedom of the lipid acyl chains adjacent to the peptides could be reduced due to a peptide−lipid interaction. Third, lipids adjacent to the peptides could be partly immobilized and their exchange frequency (and that of the pyrene molecules in this area) thus be significantly lower than in the bulk lipid matrix. In contrast, for temporin L, the values for I_e/I_m are progressively increased at increasing X_{POPG}. Likewise, at peptide:lipid molar ratios >1:6, the increment in DPH anisotropy *r* depends on X_{POPG} (Figure 5). This stoichiometry could represent a threshold concentration above which cooperative peptide insertion and rearrangements in the acidic phospholipid containing membranes take place. The single Trp residue of temporin L could promote its partitioning into the lipid bilayer (*34*), and in the presence of the acidic phospholipid, temporin L may insert deeper into the membranes or the amount of the peptide in the membranes could increase with increasing X_{POPG}. Compared to indolicidin with five Trp residues, temporin L has only a single Trp residue and one less net positive charge (Table 1). However, temporin L was more effective in quenching of the pyrene-labeled lipids in SOPC- and POPG-containing membranes. Temporin L is more hydrophobic than indolicidin and has a larger hydrophobic moment (Table 1). These properties could facilitate the insertion of temporin L into the lipid bilayer.

Our studies with pyrene-labeled lipids indicate that both temporin B and temporin L cause lipid lateral segregation in SOPC as well as in SOPC/POPG membranes, resulting in the formation of peptide-enriched microdomains. For acidic phospholipid-containing membranes, these domains could relate to the formation of pores in the bilayer. The presence of the negatively charged lipids aids in the reduction of the repulsive electrostatic forces between the positively charged peptides, thus allowing their aggregation in the membrane. More specifically, as suggested for magainin 2 and indolicidin (*15*), the peptide would first accumulate in the outer leaflet of the bilayer. After having reached a threshold surface concentration, a reorientation of peptides in the bilayer would then occur in a cooperative manner. Accordingly, high local peptide concentrations are achieved when the cationic peptides and the acidic phospholipids cosegregate on the surface of the bilayer into microdomains. The asymmetry would then relax via the formation of 'channels' or 'pores' constituted by a supramolecular aggregate of peptides and lipids, allowing the diffusion of the peptide into the inner leaflet of the bilayer. Simultaneously, the bilayer structure would be locally destabilized. Pore formation as an intermediate step in this process is conceivable as temporins have been shown to induce the release of liposome-entrapped fluorescent probes (*13*). Longer linear peptides such as magainin 2 and mellitin form pores in artificial membranes (*28, 35*), and membrane-spanning peptide channels would require a minimum length of about 23 residues. In the case of temporins, it would be particularly intriguing to discriminate the pore models proposed so far. They could form pores in a more complex way, perhaps

involving dimerization of the peptide (*9*). In contrast to magainin 2 and temporin B, temporin L and indolicidin cause vesiculation in SOPC and SOPC/cholesterol ($X_{chol} = 0.10$) giant vesicles, which could be relevant to their hemolytic activities (*36*, Simmaco, M., unpublished observation). In this context, it is of interest to compare the effects of the above antimicrobial peptides to those of mellitin, a highly hemolytic peptide isolated from the European honey bee *Apis mellifera*. The antimicrobial peptides magainin 2 and temporin B have pronounced effects on membranes containing negatively charged phospholipids while having minor impact on neutral membranes. While the hemolytic peptides temporin L and indolicidin preferentially bind to the acidic phospholipids, they also exhibit strong interactions with zwitterionic membranes. This is particularly true for temporin L, which induced pronounced vesiculation of neutral giant vesicles. Interestingly, mellitin induces a variety of morphologically different phases in zwitterionic membranes depending on the peptide:lipid ratio and the phase states of the lipids, including vesiculation of multibilayers, fusion of small lipid vesicles, and also fragmentation into disks and micelles (*37*). However, in the presence of the negatively charged phospholipid POPG, its ability to permeabilize zwitterionic phospholipid vesicles is dramatically reduced. A transbilayer orientation in neutral multilayers, but not in negatively charged multilayers, was suggested (*38*). Accordingly, these data suggest pronounced hydrophobic interactions between zwitterionic membranes and these peptides to make the latter hemolytic, while electrostatic interactions seem to be needed for their antimicrobial activity. To this end, the outer leaflet of mammalian plasma membranes is exclusively composed of zwitterionic phospholipids whereas the bacterial membrane contains significant amounts of acidic phospholipids, phosphatidylglycerol and cardiolipin (*39*).

Interestingly, all peptides studied so far in our laboratory also induce an endocytosis-like process in giant vesicles, yet the differences observed in the aggregated structures suggest different modes of association of the four peptides with membranes. The microscopy images revealed the formation of the macroscopic aggregates to be asymmetric, i.e., to occur inside the giant vesicles. Similarly to our studies on the formation of ceramide by sphingomyelinase (*21*), this vectorial nature of the action of the antimicrobial peptides suggests that their asymmetric application onto the outer surface results in an augmented bending rigidity as well as negative spontaneous curvature in the membrane. However, elucidation of the mechanism(s) requires further studies. The nature of the aggregates visible by microscopy is of interest. To this end, the possibility that the lamellar liquid-crystalline phase would not represent thermodynamic equilibrium has been proposed. Accordingly, dimyristoylphosphoglycerol has been demonstrated to transform into the so-called 'sponge' phase (*40*). The factors controlling the formation of this phase remain poorly understood; however, lipid headgroup interactions appear to be important. An intriguing possibility is that in addition to their other effects on bilayers these antimicrobial peptides could trigger a transition of the bacterial lipid phosphatidylglycerol from a lamellar liquid-crystalline state into the 'sponge' phase, the latter representing the thermodynamic equilibrium. On the level of thermodynamics, this would also provide the driving force for the macroscopic aggregation of the peptide−lipid complexes observed in giant liposomes. However, also in this case the mechanistic basis would warrant further studies.

REFERENCES

1. Boman, H. G. (1995) *Annu. Rev. Immunol. 13*, 61−92.
2. Simmaco, M., Mignogna, G., and Barra, D. (1998) *Biopolymers 47*, 435−450.
3. Mor, A., Hani, K., and Nicolas, P. (1994) *J. Biol. Chem. 269*, 31635−31641.
4. Amiche, M., Seon, A. A., Pierre, T. N., and Nicolas, P. (1999) *FEBS Lett. 456*, 352−356.
5. Bechinger, B. (1997) *J. Membr. Biol. 156*, 197−211.
6. Oren, Z., and Shai, Y. (1998) *Biopolymers (Pept. Sci.) 47*, 451−463.
7. McElhaney, R. N., and Prenner, E. J., Eds. (1999) *Biochim. Biophys. Acta 1462 (Special Issue)*, 1−234.
8. Matsuzaki, K. (2001) in *Development of novel antimicrobial agents: emerging strategies*, pp 167−176. Horizon Scientific Press, Wymondham, U.K.
9. Simmaco, M., Mignogna, G., Canofeni, S., Miele, R., Mangoni, M. L., and Barra, D. (1996) *Eur. J. Biochem. 242*, 788−792.
10. Halverson, T., Basir, Y. J., Knoop, F. C., and Conlon, J. M. (2000) *Peptides 21*, 469−476.
11. Goraya, J., Wang, Y., Li, Z., O'Flaherty, M., Knoop, F. C., Platz, J. E., and Conlon, J. M. (2000) *Eur. J. Biochem. 267*, 894−900.
12. Kim, J. B., Halverson, T., Basir, Y. J., Dulka, J., Knoop, F. C., Abel, P. W., and Conlon, J. M. (2000) *Regul. Pept. 90*, 53−60.
13. Mangoni, M. L., Rinaldi, A. C., Di Giulio, A., Mignogna, G., Bozzi, A., Barra, D., and Simmaco, M. (2000) *Eur. J. Biochem. 267*, 1447−1454.
14. Oh, H., Hedberg, M., Wade, D., and Edlund, C. (2000) *Antimicrob. Agents Chemother. 44*, 68−72.
15. Zhao, H., Mattila, J. P., Holopainen, J. M., and Kinnunen, P. K. J. (2001) *Biophys. J. 81*, 2979−2991.
16. Brockman, H. (1999) *Curr. Opin. Struct. Biol. 9*, 438−443.
17. Wiedmer, S. K., Hautala, J., Holopainen, J. M., Kinnunen, P. K. J., and Riekkola, M.-L. (2001) *Electrophoresis 22*, 1305−1313.
18. Kinnunen, P. K. J., Koiv, A., and Mustonen, P. (1993) in *Fluorescence Spectroscopy* (Wolfbeis, O. S., Ed.) pp 159−171, Springer-Verlag, New York.
19. Duportail, G., and Lianos, P. (1996) in *Vesicles* (Rosoff, M., Ed.) pp 295−372, Marcel Dekker, New York.
20. Angelova, M. I., and Dimitrov, D. S. (1986) *Faraday Discuss. Chem. Soc. 81*, 303−311.
21. Holopainen, J. M., Angelova, M. I., and Kinnunen, P. K. J. (2000) *Biophys. J. 78*, 830−838.
22. Holopainen, J. M., Penate Medina, O., Metso, A. J., and Kinnunen, P. K. J. (2000) *J. Biol.* Chem. *275*, 16484−16489.
23. Schnorf, M., Potrykus, I., and Neuhaus, G. (1994) *Exp. Cell Res. 210*, 260−267.
24. Lentz, B. R. (1993) *Chem. Phys. Lipids. 64*, 99−116.
25. Lehtonen, J. Y. A., and Kinnunen, P. K. J. (1994) *Biophys. J. 66*, 1981−1990.
26. Holopainen, J. M., Lehtonen, J. Y. A., and Kinnunen, P. K. J. (1997) *Chem. Phys. Lipids 88*, 1−13.
27. Eisenberg, D. (1984) *Annu. Rev. Biochem. 53*, 595−623.
28. Matsuzaki, K. (1999) *Biochim. Biophys. Acta 1462*, 1−10.
29. Ladokhin, A. S., Selsted, M. E., and White, S. H. (1999) *Biochemistry 38*, 12313−12319.
30. Ha, T. H., Kim, C. H., Park, J. S., and Kim, K. (2000) *Langmuir 16*, 871−875.
31. Pathak, N., Salas-Auvert, R., Ruche, G., Janna, M. H., McCarthy, D., and Harrison, R. G. (1995) *Proteins: Struct., Funct., Genet. 22*, 182−186.
32. Kinnunen, P. K. J., Koiv, A., Lehtonen, J. Y., Rytomaa, M., and Mustonen, P. (1994) *Chem. Phys. Lipids 73*, 181−207.
33. Dougherty, D. A. (1996) *Science 271*, 163−168.

34. Wimley, W. C., and White, S. H. (1996) *Nat. Struct. Biol. 3*, 842−848.
35. Bechinger, B. (1999) *Biochim. Biophys. Acta 1462*, 157−183.
36. Ahmad, I. W., Perkins, R., Lupan, D. M., Selsted, M. E., and Janoff, A. S. (1995) *Biochim. Biophys. Acta 1237*, 109−114.
37. Dufourcq, J., Faucon, J. F., Fourche, G., Dasseux, J. L., Le Maire, M., and Gulik-Krzywicki, T. (1986) *Biochim. Biophys. Acta 859*, 33−48.
38. Ladokhin, A. S., and White, S. H. (2001) *Biochim. Biophys. Acta 1514*, 253−260.
39. Op den Kamp, J. A. (1979) *Annu. Rev. Biochem. 48*, 47−71.
40. Schneider, M. F., Marsh, D., John, W., Kloesgen, B., and Heimburg, T. (1999) *Proc. Natl. Acad. Sci. U.S.A. 96*, 14312−14317.

BI011929E